Acta Materialia 185 (2020) 181–192

Contents lists available at ScienceDirect

Acta Materialia

journal homepage: www.elsevier.com/locate/actamat

Full length article

Ultra-high strength and plasticity mediated by partial dislocations and defect networks: Part I: Texture effect

Ruizhe Su[a], Dajla Neffati[b], Qiang Li[a], Sichuang Xue[a], Jaehun Cho[a], Jin Li[a], Jie Ding[a], Yifan Zhang[a], Cuncai Fan[a], Haiyan Wang[a], Yashashree Kulkarni[b,*], Xinghang Zhang[a,*]

[a] School of Materials Engineering, Purdue University, West Lafayette, IN 47907, USA
[b] Department of Mechanical Engineering, University of Houston, Houston, TX 77204, USA

ARTICLE INFO

Article history:
Received 24 May 2019
Revised 2 November 2019
Accepted 18 November 2019
Available online 20 November 2019

Keywords:
Multilayers
Twin boundaries
Stacking faults
Phase transformation
Molecular dynamic simulations

ABSTRACT

Deformation mechanisms governing the strength of nanostructured metallic multilayers have been studied extensively. In general, size effect is the most effective way to tailor the mechanical strength of multilayers. Here we report that three Cu/Co multilayer systems with identical layer thickness but different types of layer interfaces exhibit drastically different mechanical behavior. *In situ* micropillar compression tests inside a scanning electron microscope show that coherent FCC (100) and (110) Cu/Co multilayer systems have low yield strength of about 600 MPa, and prominent shear instability. In contrast, the incoherent Cu/ HCP Co multilayers show much greater yield strength, exceeding 2.4 GPa, and significant plasticity manifested by a cap on the deformed pillar. Molecular dynamics simulations reveal an unexpected interplay among pre-existing twin boundaries in Cu, stacking faults in HCP Co, and incoherent layer interfaces, which leads to partial dislocation dominated high strength and outstanding plasticity. This study provides fresh insights for the design of strong, deformable nanocomposites by using a defect network consisting of twin boundaries, stacking faults and layer interfaces.

1. Introduction

Nanostructured metallic multilayers have drawn significant attention because of their high strength, good wear resistance, resilient radiation tolerance, and intriguing magnetic properties for a variety of potential applications in industry [1–11]. In terms of mechanical properties, previous studies have mostly focused on the layer thickness (h) and layer interface dependent strengthening and deformation mechanisms in different systems, such as FCC/FCC [1,11-16], FCC/HCP [2,6,17,18], FCC/BCC [6,9,11,18–23, HCP/HCP [24], HCP/BCC [25,26], metal/ceramic [27-29], and metal/amorphous [3,30–32] multilayers, where FCC, BCC and HCP stand for face-center cubic, body-center cubic and hexagonal close packed crystal structures. Some of the key layer thickness (size) dependent strengthening mechanisms are briefly summarized as follows [33]: when h is greater than 50 nm, strengthening due to dislocation pile-ups against layer interfaces follows the Hall-Petch relationship; when h is between 5 nm and 50 nm, deformation mechanism transitions to confined layer slip (CLS), where single dislocation loops can glide between layer interfaces; and when h is less than 5 nm, multilayers often reach their maximum strength, which is determined by the resistance of the interfaces to the transmission of single dislocations. In general, coherent interfaces, such as those in Cu/Ni, are weak barriers to transmission of dislocations [11,12], whereas incoherent interfaces, such as those in Cu/Nb, are stronger dislocation barriers due to slip discontinuity [6,9,11].

Nanostructured metallic multilayers are known for their high strength, testified by nanoindentation [2,12,14,15,19] and micropillar compression [3,17,20,24,28,34-36] studies. However, most high strength multilayers show shear instability under compression (formation of shear bands or cracks) [9,16,18,20,22,23,26,29,37]. There are abundant studies on the extrinsic (pillar diameter d) and intrinsic (layer thickness h) size effects on toughening in metallic multilayers. These studies show that by increasing d or h, multilayer pillars show more 'ductile' (uniform deformation or barreling) deformation, but doing so also leads to softening. There are few studies that focus on the influence of texture on the strength and deformability of multilayers with chemically identical layer constituents and layer thickness.

Here we report on *in situ* micropillar compression studies of highly textured Cu 25 nm/Co 25 nm (referred as Cu/Co 25 nm hereafter) multilayers with three different crystallographic orientations, {100}, {110} and FCC {111}/HCP {0002} textures and significantly different layer interfaces. The *in situ* studies reveal the surpris-

* Corresponding authors.
E-mail addresses: ykulkarni@uh.edu (Y. Kulkarni), xzhang98@purdue.edu (X. Zhang).

https://doi.org/10.1016/j.actamat.2019.11.049
1359-6454/

ingly high yield strength of {111} textured multilayers, exceeding 2.4 GPa, compared to ~ 600 MPa yield strength for both {100} and {110} textured multilayers. Molecular dynamics (MD) simulations reveal that the semicoherent {100} and {110} layer interfaces have low resistance to the transmission of partial dislocations, whereas {111} textured Cu/Co nanolayer has a defect network consisting of twin boundaries in FCC Cu, stacking faults (SFs) in HCP Co, and the incoherent layer interface, thus offering high strength by prohibiting the propagation of partials. Furthermore the FCC {111}/HCP {0002} multilayers have large deformability due to the superplastic deformation of the pillar cap layer, which arises from detwinning and HCP-to-FCC Co phase transformation induced softening. This study provides an important concept, that is tailoring the network of planar defects can lead to the design of ultra-high strength, deformable nanocomposites for a variety of industrial and defense applications.

2. Experimental and simulation methods

2 μm thick Cu/Co 25 nm multilayers were deposited on HF etched Si (100), Si (110) and Si (112) substrates with 100 nm Cu seed layers using DC magnetron sputtering. The base pressure of the sputter chamber was 5×10^{-6} Pa and the deposition rates were ~0.5 nm/s for Cu and ~0.15 nm/s for Co. X-ray diffraction (XRD) experiments were performed by using a Bruker D8 Discover X-ray powder diffractometer at room temperature. Transmission electron microscopy (TEM) and high resolution TEM (HRTEM) experiments were performed on an FEI Talos 200X transmission electron microscope operated at 200 kV. *In situ* micropillar compression tests were performed by using Hysitron PI 88xR PicoIndenter inside an FEI Quanta 3D FEG dual-beam scanning electron microscope. Cu/Co multilayer pillars with ~1 μm in diameter and ~2 μm in height were fabricated using the same scanning electron microscopy (SEM) microscope equipped with focused-ion-beam (FIB). The height-to-diameter aspect ratio was kept at about 2:1 for the micropillars, following the general consensus within the community [38-40].

Three cylindrical nanopillars of Cu/Co multilayers with {100}, {110} and {111} /{0002} crystallographic structures, respectively, were studied by performing MD simulations using LAMMPS [41]. For FCC (100) and (110) pillars, the thickness of each layer is 5.3 nm, the total specimen height is about 32 nm and the diameter is ~19 nm. For Cu (111)/Co (0002) pillars, the thickness of each layer is 5 nm, the total specimen height is ~30 nm and the diameter is about 15 nm. The aspect ratio of the FCC pillars is 1:1.7 and that of the FCC Cu/HCP Co pillar is 1:2. The simulations were performed at 300 K under the NVT canonical ensemble. The interactions between Cu and Co were modeled by the embedded-atom method (EAM) potential developed by Zhou et al. [7]. The potential was validated by calculating the elastic constants and the stacking fault energies for Cu as well as Co. The values were found to be in reasonable agreement with experimental results as well as simulations performed using another EAM potential for HCP and FCC Co developed by Mishin et al. [42]. Non-periodic boundary conditions were used in all directions. First, conjugate gradient energy minimization was performed, followed by equilibration of the specimens at 300 K. Then, the specimens were subjected to compression at a constant strain rate. The FCC (100) and (110) pillars were subjected to compression for 800 ps at a strain rate of 1.66×10^8 s^{-1}. Cu (111)/Co (0002) pillars were subjected to compression for 900 ps at a strain rate of 1.86×10^8 s^{-1}. The HCP/FCC multilayer specimens were created layer by layer in order to introduce pre-existing coherent twin boundaries (CTBs) in the FCC Cu layers and SFs in the Co layers parallel to the basal plane, to be consistent with the experimental specimens. The defect structures were visualized using OVITO [43].

3. Results

XRD patterns of Cu/Co 25 nm multilayers on different substrates reveal highly textured FCC Cu/Co (100) on Si (100) (Fig. 1a), FCC Cu/Co (110) on Si (112) (Fig. 1f) and Cu (111)/Co (0002) on Si (110) (Fig. 1k). Schematics in supplementary Fig. S1 show crystallographic orientation relationships between Cu, Co and Si substrates. Cu/Co multilayers deposited on Si (100) and Si (112) substrates have FCC Co, while HCP Co (0002) forms on Si (110) substrate. Cross-section EDS analyses show chemically abrupt Cu/Co layer interfaces (Fig. 1b,g,l). It is worth mentioning that all films were deposited simultaneously with the same parameters, so the dramatic microstructure differences among three Cu/Co multilayers arise mainly from different Si substrates. Cross-section TEM micrographs in Fig. 1c-e show that the FCC Cu/Co (100) multilayer contains high-density inclined SFs in the FCC Co layers, but has little defects in Cu layers. However in FCC Cu/Co (110) multilayers, besides the inclined SFs in the Co layers, coherent twin boundaries (CTBs) with ~60 nm twin spacing (see statistical analysis in supplementary Fig. S2) are also observed as confirmed by the selected area diffraction (SAD) pattern in Fig. 1h. CTBs are initiated from Cu/Si interface (Fig. 1i). In contrast to SFs confined within the Co layers, CTBs often penetrate across {110} Cu/Co interfaces throughout the entire film thickness. Few grain boundaries are observed in both {100} and {110} textured multilayers, indicating the epitaxial growth of FCC Cu/Co multilayers. However, Cu (111)/Co (0002) films deposited on Si (110) substrates show dramatically different microstructures. Instead of FCC stacking, HCP Co (0002) grows on top of the Cu (111) as confirmed by the diffraction pattern (Fig. 1m). Domain boundaries (columnar grain boundaries in epitaxial films) and curved Cu/Co layer interfaces (Fig. 1n) are formed due to island growth and coalescence. Similar domain boundaries have been observed in a previous study on epitaxial growth of nanotwinned Cu [44]. The average domain size is ~ 40 nm. High-density SFs on basal planes in the HCP Co layers and CTBs in the Cu layers are observed (Fig. 1m,o). The three types of defects, SFs-TBs-incoherent layer interfaces, thus, form a defect network. Twin spacing in Cu layer is ~8 nm (see statistical analysis in supplementary Fig. S3) and SF spacing in Co layer is ~5 nm. The defect network formed in Cu (111)/Co (0002) multilayers is a result of epitaxial growth. Our previous studies have shown that nanotwinned Cu (111) films grow epitaxially on Si (110) substrate [44]. Also HCP Co (0002) film with high-density SFs forms on Si (110) substrate [45]. Given the small lattice mismatch between Cu (111) and Co (0002) (as shown in Fig. 1k), highly textured Cu (111) / Co (0002) films form on Si (110) substrate. Consequently the Cu (111)/Co (0002) multilayer contains the defect network consisting of parallel CTBs (in Cu), SFs (in Co) and incoherent Cu/Co layer interfaces.

Mechanical behavior of Cu/Co multilayers is studied by *in situ* SEM pillar compression tests. Fig. 2a shows the true stress-strain curves for FCC Cu/Co (100) (blue and light blue) and Cu/Co (110) (orange and yellow) pillars respectively under compression at a constant strain rate (5×10^{-3}/s). Both multilayer systems yield at ~600 MPa. However, FCC Cu/Co (110) pillars show a more prominent strain hardening with a maximum flow stress of about 1 GPa. On the other hand, the maximum flow stress for FCC Cu/Co (100) pillars is ~800 MPa. Fig 2c shows SEM snapshots of a deformed FCC Cu/Co (100) pillar (with respect to the blue curve) during compression (see supplementary video 1 for details). One major slip band is nucleated at 10% strain (Fig. 2c3), and the angle between the slip band and the lateral (100) plane is ~55° In the deformed FCC Cu/Co (110) pillar shown in Fig. 2d2-d4, the first slip band emerges at ~8% strain, followed by the continuous formation of multiple parallel slip bands (See supplementary video 2 for details). The angle between the slip band and the lateral (110) plane

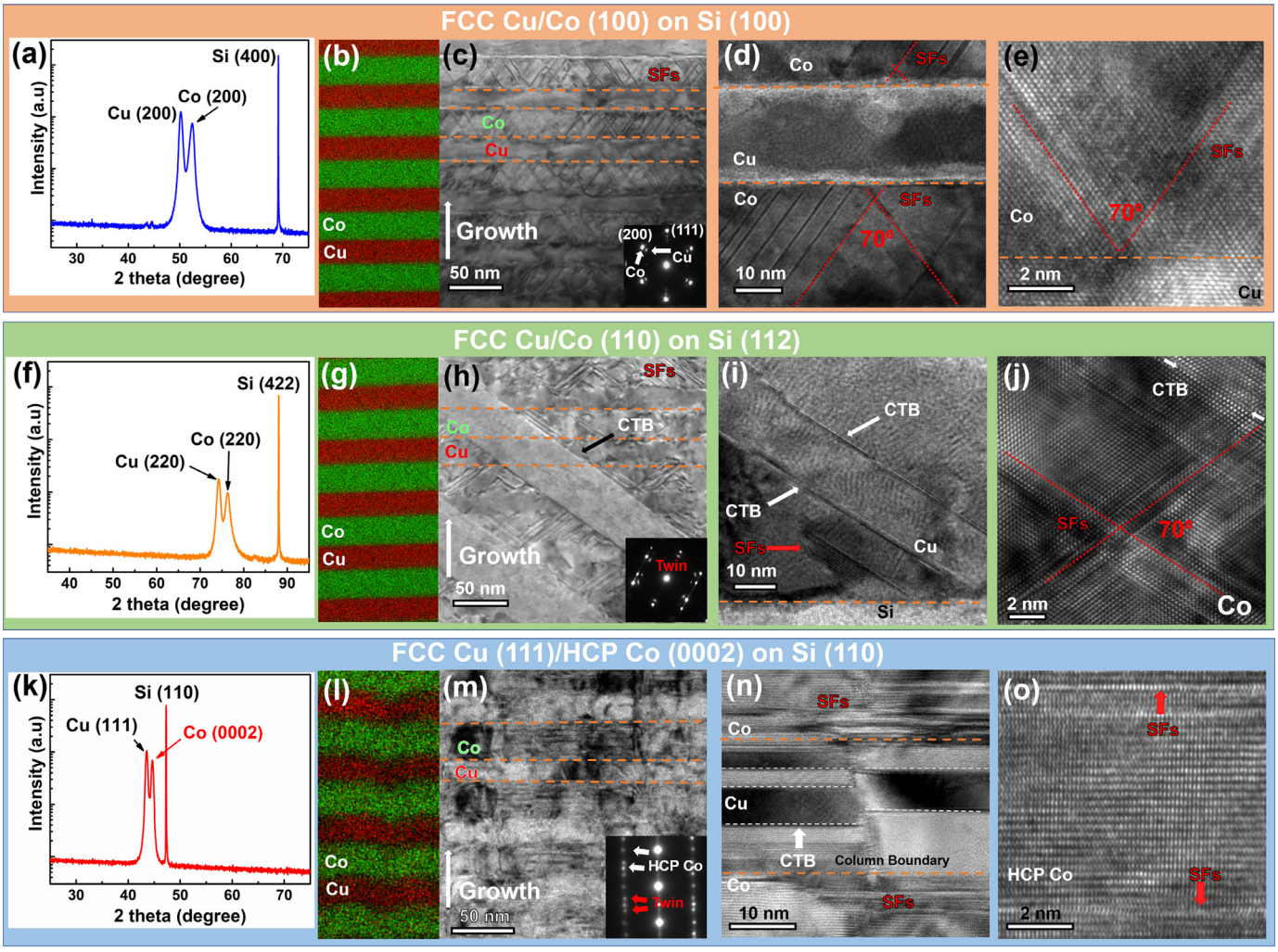

Fig. 1. Comparison of the microstructures of three Cu/Co 25 nm multilayers with different types of layer interfaces. (a, f, k) XRD profiles show the formation of epitaxial FCC Cu (100) /Co (100) interface on Si (100) substrate, FCC Cu (110) /Co (110) interface on Si (112) substrate; and highly textured Cu (111)/Co (0002) film on Si (110) substrate. (b, g, l) Cross-section EDS maps of Cu/Co nanolayers showing Co in green and Cu in red. (c-e) Cross-section TEM (XTEM) micrographs showing epitaxial FCC Cu/Co (100) interface and the formation of inclined SFs in Co layer. (h-j) XTEM micrographs showing the epitaxial semi-coherent FCC Cu/Co (110) interfaces, SFs in FCC Co and CTBs penetrating across the Cu/Co interface. (m-o) XTEM micrographs showing the coexistence of parallel defect networks, consisting of incoherent Cu (111)/Co (0002) interfaces, high-density SFs in HCP Co and CTBs in Cu. (For interpretation of the references to color in this figure, the reader is referred to the web version of this article.)

is 35° Note that the slip bands in the FCC (100) and (110) pillars are both parallel to the {111} planes.

In contrast to the two FCC multilayer systems, compression tests on the Cu (111)/Co (0002) pillars reveal drastically different mechanical behavior as shown in Fig. 2b. (Supplementary Fig. S4 shows reproducibility of deformed multilayer pillars). Due to the non-uniform deformation of the Cu (111)/Co (0002) pillar, we compare the engineering stress-strain curves for all three systems. As shown in Fig. 2b, the Cu (111)/Co (0002) pillars (red and pink) show a dramatically higher yield strength, ~2.4 GPa, which is 4 times that of the two FCC Cu/Co systems and the flow stress exceeds 3 GPa. The average true stress-strain curve for the deformed cap layer in Cu (111)/Co (0002) pillar (shown in supplementary Fig. S5) still shows that Cu (111)/Co (0002) has the greatest flow stress, ~ 3 GPa, among all the three multilayer systems and reveals significant work hardening up to ~ 19% strain, before substantial softening occurs. SEM snapshots in Fig. 2e show the significant extrusion of the pillar top, as evidenced by the formation of a 200 nm-thick pancake shaped cap, while the bottom part of the pillar remains largely unchanged as shown in Fig. 2e4 (See supplementary video 3 for details). The flow stress is one of the highest among all multilayers tested by micropillar compression to date (Supplementary Fig. S6) [3,9,16–18,20-24,26-30,37,46–48]. Besides, we compare the flow stress between Cu/Co multilayers with other multilayer systems showing 'ductile' deformation behavior (no shear band or crack formation) under pillar compression (see supplementary Fig. S7 for a summary of deformed pillar morphology) and plot the comparisons as a function of $h^{-1/2}$ in Fig. 3. Cu (111)/Co (0002) multilayer has the highest flow stress ~3 GPa among all 'ductile' multilayer pillars reported to date. To exclude the effect of residual stress on the different mechanical properties of Cu/Co multilayers, we measured the curvature of Si substrates before and after deposition, and calculated the residual stress as shown in supplementary Table S1. The tensile residual stresses for the three Cu/Co multilayers are similar, ~410–570 MPa. Thus, the residual stress cannot explain the significant difference in mechanical strength among three multilayer systems measured during *in situ* compression tests. The strengthening and toughening mechanisms will be discussed in detail below.

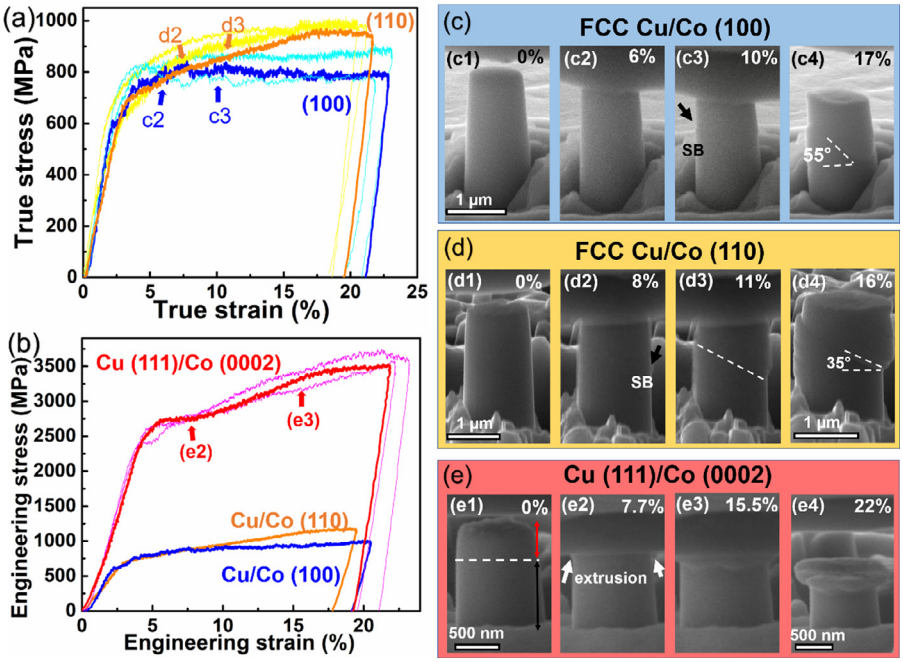

Fig. 2. *In situ* micropillar compression tests for the three Cu/Co 25 nm multilayer systems obtained at identical strain rate (5×10^{-3}/s). (a) True stress-strain curves show that Cu/Co (100) and (110) multilayers both have a yield strength of ~600 MPa, while Cu/Co (110) shows a more prominent strain hardening. (b) Engineering stress-strain curves show that Cu (111)/Co (0002) pillars have a significantly higher yield strength, ~2400 MPa than other two systems. (c1-c4) SEM snap shots of Cu/Co (100) show a uniform deformation before 10% strain followed by the formation of a major slip band (SB) at ~55° angle with respect to the (100) plane. (d1-d4) SEM images of Cu/Co (110) show that the first slip band starts to form at 8% strain, and multiple slip bands at ~35° angle with respect to the (110) plane are formed after 10% strain. (e1-e4) SEM images of Cu (111)/Co (0002) show significant plastic deformation accumulated primarily at the top portion (~500 nm) of the pillar, forming a cap, while the rest of the pillar remains largely unchanged. (See supplementary video 1–3 for details). (For interpretation of the references to color in this figure, the reader is referred to the web version of this article.)

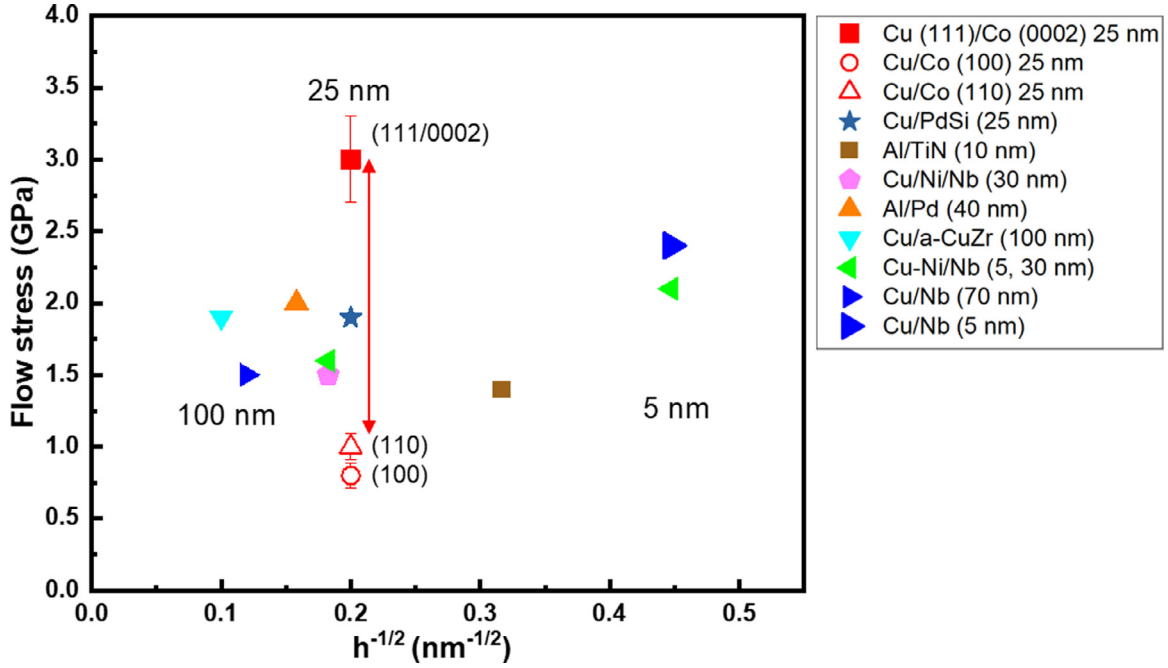

Fig. 3. Comparison of flow stress between Cu/Co 25 nm multilayers with other 'ductile' deformed multilayers under pillar compression: Cu/PdSi (25 nm) [3], Al/TiN (10 nm) [27], Cu/Ni/Nb (30 nm) [47], Al/Pd (40 nm) [16], Cu/a-CuZr [17], Cu-Ni/Nb (5, 30 nm) [47] and Cu/Nb (5 [9], 70 nm [48]). Flow stress is taken from the true stress at 5–10% true strain. All solid data points come from pillars deformed in a ductile way. Open data points are from Cu/Co with different texture from this study. The flow stress of Cu/Co (0002) 25 nm system is the highest among all ductile metallic nanolayers reported to date, and is significantly higher than that of (100) and (110) Cu/Co 25 nm nanolayers.

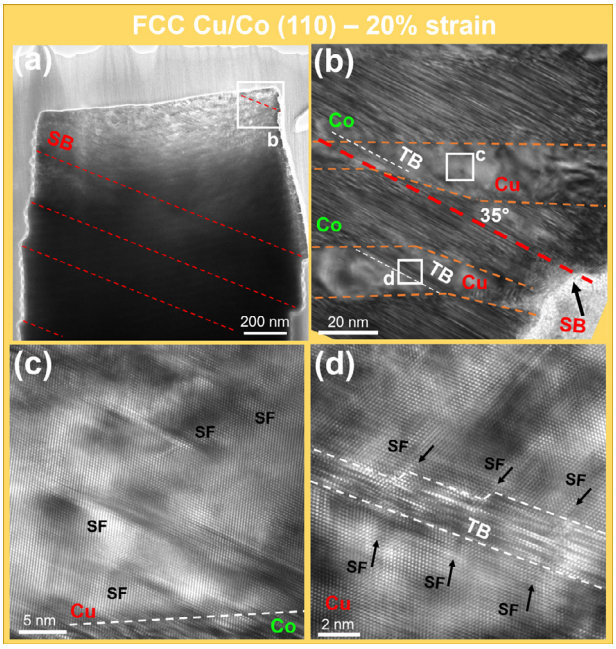

Fig. 4. XTEM micrographs of the FCC (110) Cu/Co 25 nm pillar after compression. (a) Multiple slip bands (SB) are formed after deformation. (b) Slip bands are formed along the pre-existing TBs. The inclined SFs in the Co layer are also parallel to the TBs. (c-d) HRTEM micrographs show SFs, and thickened TBs in Cu layers. The slip bands and SFs in Co and Cu layer are all parallel to the CTBs, indicating that {111} planes along CTBs become the preferred glide planes for dislocations. Rather than one major slip band observed in the deformed (100) Cu/Co pillar, multiple slip bands formed in the deformed (110) Cu/Co system. HRTEM micrograph in Fig. 4c shows SFs in a Cu layer, which were not observed before deformation. These SFs formed due to the transmission of Shockley partials across layer interfaces.

4. Discussion

4.1. Strain hardening and deformation mechanisms in FCC CU/CO multilayers

Size dependent strengthening has been well documented in metallic multilayers. In this study, the layer thickness h is 25 nm for all samples, a regime where CLS is normally the dominant deformation mechanism, although dislocation pile-ups cannot be entirely suppressed [49]. Experimentally, instead of the extrusion of the soft Cu layers, slip bands were observed in both FCC (100) and (110) Cu/Co pillars (Fig. 2c,d), indicating that CLS may not be the preferred deformation mode. TEM micrographs of a deformed (110) Cu/Co pillar (Fig. 4c, d) show the formation of SFs in a Cu layer, which were not observed before deformation. These SFs formed due to the transmission of Shockley partials across layer interfaces. The transmission of single dislocations through coherent Cu/Co interface along {111} glide planes may determine the yield strength of the multilayers [33,50]. The interface barrier strength can be expressed as follows:

$$\tau_{int} \approx \tau_K + \tau_{ch}, \tag{1}$$

where τ_{int} is the interface barrier resistance, τ_K is Koehler stress originating from modulus mismatch, and τ_{ch} is the chemical interaction term related to SFE (stacking fault energy) difference between layer constituents [50]. τ_K can be described by

$$\tau_K = \frac{\mu_1(\mu_2-\mu_1)b}{4\pi(\mu_1+\mu_2)l}, \tag{2}$$

where μ_1 and μ_2 are the shear modulus of Cu and Co, b is Burgers vector, l is dislocation core size, ~2–4 b. The calculated τ_K is ~ 170–330 MPa for both FCC systems. Additionally,

$$\tau_{ch} = \frac{\gamma_2-\gamma_1}{b}, \tag{3}$$

where γ_1 and γ_2 are respective SFE of Cu and Co.

$$\sigma = \frac{\tau_{int}}{\cos\phi\cos\lambda}. \tag{4}$$

In FCC (100) and (110) multilayers, ϕ or λ are complementary to each other, thus the two epitaxial systems should have similar yield strength, calculated as 520~870 MPa, which is comparable to experimentally measured yield strength, ~ 600 MPa for both systems.

Next, we examine the difference in strain hardening ability between the two FCC multilayers. A major microstructure difference between the two FCC systems is the frequently observed giant CTBs running inclined across the layer interfaces in the FCC Cu/Co (110) film. The average twin spacing of CTBs is ~60 nm. CTBs are known as effective dislocation barriers and contribute to strengthening and work hardening [44,51-56]. TEM micrographs of a deformed (110) Cu/Co pillar (Fig. 4d) show a thickened CTB with SF decorations on both sides. CTBs decorated with SFs have been predicted in simulation [53,57,58] and observed experimentally [55,59], resulting from interaction between the gliding partials and CTBs. The CTBs block the propagation of partials, leading to strengthening and work hardening [44,51-56].

MD simulation results for nanopillar compression of (100) and (110) Cu/Co 5 nm multilayers also support our conjecture. True stress-strain curves (Fig. 5a,b) reveal higher flow stress in FCC Cu/Co (110) nanopillar. For the FCC Cu/Co (100) nanopillar, Shockley partials transmit through the Cu/Co interface (Fig. 5c) near the onset of yielding, leading to penetration of SFs across the interface (Fig. 5c). During plastic deformation, the glide of Shockley partials and consequent propagation of SFs dominate the deformation, and slip bands form from the surface of the pillar as shown in Fig. 5d. Supplementary video 4 shows three parallel videos for the simulated deformation of Cu/Co (100) system. The left panel shows the true stress-strain plot; the middle panel reveals the evolution of SFs and the atoms are colored following the nearest neighbor analysis; the right panel shows the evolution of chemically abrupt Cu (red) and Co (green) layers during deformation. Also in supplementary video 5, only SFs (purple) and dislocations are shown. Green lines denote Shockley partials, yellow lines denote Hirth lock, blue lines denote perfect dislocations and red lines denote other dislocations. Similarly in the FCC Cu/Co (110) pillar, Shockley partials migrate across the Cu/Co interface, leading to plastic yielding (Fig. 5e). Furthermore, CTBs formed in FCC (110) pillar during deformation block the transmission of partials, and consequently contribute to work hardening. The substantial softening (manifested as the stress-drop in Fig. 5b) arises from the transmission of Shockley partials across the CTBs as shown in Fig. 5f (See supplementary Fig. S8, video 6 and 7 for more details). Although the multilayers in MD simulations only have 5 nm individual layer thickness, these findings reveal that the coherent (100) and (110) FCC Cu/Co interfaces are weak dislocation barriers, and thus the strength and plasticity of these coherent systems are dominated by the glide and transmission of partial dislocations across layer interfaces.

4.2. Origins of ultra-high strength and plasticity in Cu (111)/Co (0002) multilayer system

The Cu (111)/Co (0002) 25 nm multilayer is the strongest ductile metallic multilayer reported to date as shown in Fig. 3. Cu/W 20 nm multilayer has higher flow stress, but it failed in a brittle way (supplementary Fig. S9c). The yield strength and flow stress

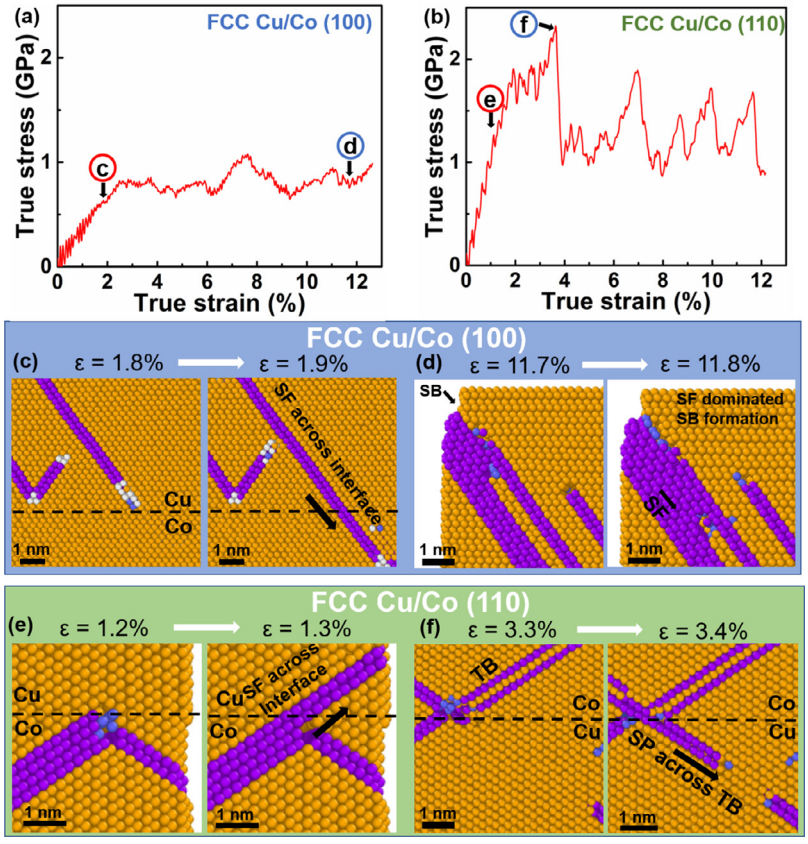

Fig. 5. Comparison of MD simulation results for the FCC (100) and (110) Cu/Co 5 nm multilayer nanopillars. (a) The FCC (100) Cu/Co multilayer shows a flow stress of ~ 0.8–1 GPa. (b) The FCC (110) Cu/Co multilayer has a flow stress of ~ 1–2 GPa. (c) Microstructure and dislocation analyses of FCC (100) multilayer at 1.8–1.9% strain show SFs penetrating through the layer interface, corresponding to the onset of plastic yielding shown in Fig. 5a. Atoms are in common neighbor color coding where orange, purple and white denote FCC, HCP and unidentified structures, respectively. (d) In the FCC Cu/Co (100) pillar deformed to a strain of 11.7%, Shockley partials glide mostly on one set of {111} planes, causing the formation of a slip band (SB). (e) In the FCC (110) Cu/Co pillar deformed to 1.2–1.3% strain, SFs penetrate through the Cu/Co layer interface. (f) At a strain of 3.4%, SFs in the FCC Cu/Co (110) pillar penetrate through TBs, leading to substantial softening. (See supplementary video 4 and 5 for details). (For interpretation of the references to color in this figure, the reader is referred to the web version of this article.)

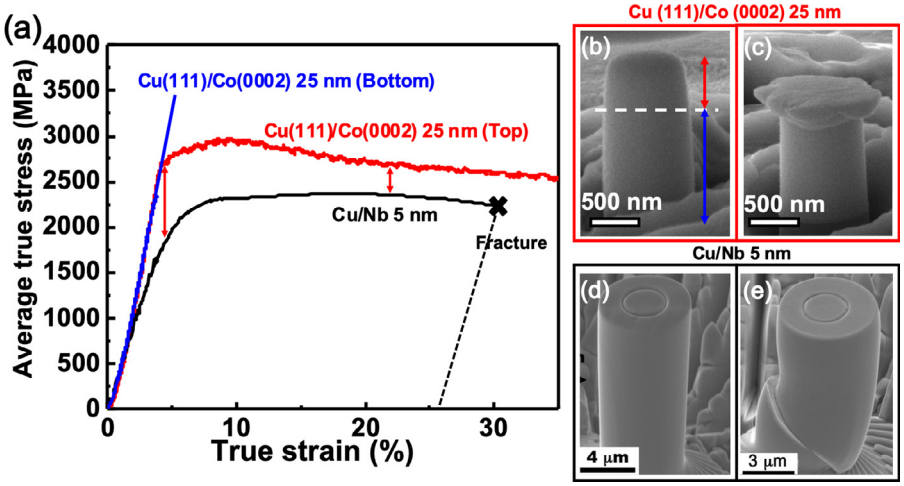

Fig. 6. Comparison of *in situ* micropillar compression tests of Cu (111)/Co (0002) 25 nm multilayer with Cu/Nb 5 nm multilayers. (a) True stress-strain curves of Cu/Nb 5 nm multilayers [9] showing 1.8 GPa yield strength and 2.4 GPa flow stress. (b,c) SEM micrographs of Cu (111)/Co (0002) pillars showing substantial plastic deformation on the top part of pillar. (d,e) SEM micrographs showing a major shear band generated during compression for Cu/Nb 5 nm pillar at a strain of 28%.

of Cu (111)/Co (0002) 25 nm multilayer are also much higher than the benchmark values of Cu/Nb 5 nm multilayer [9] (Fig. 6). In addition, the Cu/Nb 5 nm pillar forms a major shear band after compression to a strain of 28%; whereas the Cu/Co 25 nm pillar forms a large spherical cap, and sustains up to 90% of true strain without the formation of shear band induced fracture.

The significant yield strength discrepancy between the two FCC Cu/Co systems and Cu (111)/Co (0002) multilayers originates from their different microstructures. Compared with FCC Cu/Co multilayers, the Cu (111)/Co (0002) multilayers have a defect network, containing three types of mutually parallel planar defects: CTBs in Cu, SFs in Co, and incoherent FCC/HCP layer interfaces.

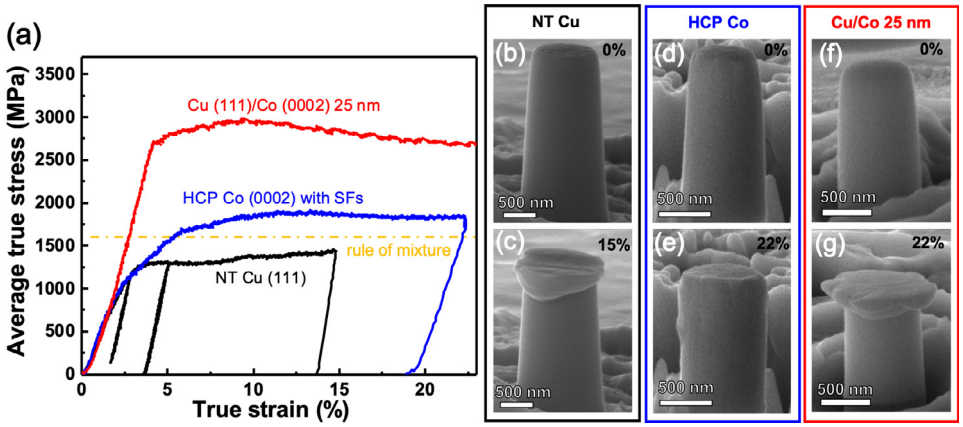

Fig. 7. *In situ* compression tests of nanotwinned (NT) Cu, HCP Co with stacking faults and Cu (111)/Co (0002) 25 nm nanolayers. (a) Average stress-strain plots showing the flow stress of NT Cu and HCP Co with SFs are 1.2 GPa and 1.7 GPa respectively, which are much lower than the flow stress of Cu (111)/Co (0002) 25 nm multilayers. (b-c) SEM micrographs showing the substantial deformation near pillar top for NT Cu. (d-e) SEM micrographs showing uniform deformation for HCP Co pillar (f-g) SEM micrographs showing the substantial deformation near pillar top for Cu (111)/Co (0002) 25 nm multilayers. These comparison studies confirm that the high strength and significant deformability in Cu (111)/Co (0002) multilayers do not arise from twins or SFs alone. Instead the defect networks, containing incoherent interface + twins + SFs, must operate in a collaborative way to achieve high strength and significant plasticity.

We start the discussion with CTBs. Dislocation interactions with TBs may have a hard mode and an easy mode [59,60]. CTBs are shown to be effective barriers for the transmission of dislocations on the inclined slip systems, resulting in the hard deformation mode [44,52,53,55,56,61-63]. However, in *situ* tensile testing of nanotwinned Cu [59] has revealed that when TB spacing is below 10 nm, dislocation glide along CTBs becomes the dominant deformation mechanism, and the stress required to activate partial migration is low, leading to softening observed in nanotwinned metals with small twin spacing. Although the twin spacing in Cu is less than 10 nm, during the uniaxial compression test of Cu (111)/Co (0002) pillar, there is no resolved shear stress for the migration of partials along CTBs, and thus we anticipate a high yield strength for the plastic yielding of nanotwinned Cu.

Secondly, the easy glide plane in HCP Co is the {0002} basal plane [64,65], which is also normal to the loading direction in this study. At the same time, the activation of ⟨c⟩ and/or ⟨$c+a$⟩ dislocations on the pyramidal or prismatic slip planes may be blocked by high-density SFs [66], consequently increasing the yield strength of HCP Co.

Third, unlike the coherent FCC Cu/Co interfaces, the incoherent FCC/HCP layer interface is another strong barrier for dislocation transmission. Dislocations in Cu layers may be difficult to transmit through the incoherent interface due to slip discontinuity in FCC Cu and HCP Co. To sum up the aforementioned rationale, the inclined slip of dislocations and the propagation of slip bands are prohibited by a defect network, consisted of the nanotwins in Cu, high-density SFs in Co, and the incoherent FCC/HCP interfaces, and consequently we may obtain ultra-high strength in the FCC Cu/HCP Co nanolayers. We also compared the *in situ* pillar compression results on pure HCP Co with high density SFs on basal plane [45] and nanotwinned Cu with similar defects density [67], and their flow stresses are both less than 2 GPa with a rule-of-mixture flow stress of 1.5 GPa (Fig. 7). These comparisons indicate that the ultra-high strength of Cu (111)/Co (0002) multilayers arises from the TB-SF-interface defect network, rather than from any type of stand-alone defects. This hypothesis is tested and the mechanisms for the onset of plastic yielding of these high strength nanolayer composites are investigated further through post-compression TEM studies and MD simulations as discussed below.

EDS maps of Cu (111)/Co (0002) pillars deformed to a compressive strain of 5% in Fig. 8a1-a2 show the prominent dilation of the pillar top. Significant plasticity and even local superplasticity are evident near the heavily deformed regions in both Cu and Co layers. HRTEM micrograph in Fig. 8a3 shows steps and SFs on CTBs in Cu. CTBs in as-deposited multilayers are mostly sharp boundaries, and hence the steps on CTBs form presumably due to partial dislocation-TB intersections, similar to what has been observed previously [68,69]. The steps on the TBs are also active sources for the emission of mobile Shockley partials, promoting plasticity during deformation. In the deformed HCP Co layers (Fig. 8a4), phase transformation from HCP to FCC phase is observed, which may be triggered by high local stresses [70-72]. In the pillar deformed to 20% of strain, significant co-deformation of Cu and Co to more than 90% has been observed in the top of the pillar as shown by the EDS maps in Fig. 8b1-b2. Furthermore, the serious expansion of the cap layer leads to the formation of a unique “T-shirt” type of cross-sectional morphology, indication of giant plasticity in the cap. Significant detwinning is observed in the Cu layer (Fig. 8b3); and an extremely high density of SFs is observed in the Co layer in the “shoulder of the T-shirt” (Fig. 8b4). The formation of extremely high density of SFs in the HCP Co may be related to the rotation of the layers and the increase of Schmidt factor that facilitate the migration of partials on the basal plane of the HCP Co. FCC Co was the dominant phase in the center of the pillar cap. When HCP Co is transformed to an FCC crystal structure, as mentioned earlier, the FCC Cu/FCC Co interface is transparent to dislocation migration, and partial dislocations can easily glide on the inclined {111} planes.

MD simulations of compression on Cu (111)/Co (0002) multilayer with pre-existing nanotwins in Cu and SFs in Co (Fig. 9a-c) reveal the atomistic mechanisms of high strength and significant plasticity. Briefly speaking, the horizontal CTBs in Cu layer, SFs in HCP Co and incoherent layer interfaces all prohibit the penetration of dislocations, and thus the defect networks consisting of TB-SF-layer interfaces lead to ultra-high strength in Cu/Co nanolayers with FCC/HCP layer interfaces.

The yield strength of the nanopillar is found to be ~5.5 GPa, much higher than that of the two simulated FCC Cu/Co multilayers. Before yielding, Shockley partials are nucleated from Cu/Co interface and glide long the inclined {111} planes, interact and transmit across the CTBs in Cu (Fig. 9d), leading to steps on the CTBs [53,58,69,73]. These steps trigger the onset of detwinning in Cu via the migration of Shockley partials along CTBs. Note that the microscopic yielding in the Cu layer does not lead to the significant stress-drop in the stress-strain curve (Fig. 9a). In Co layer,

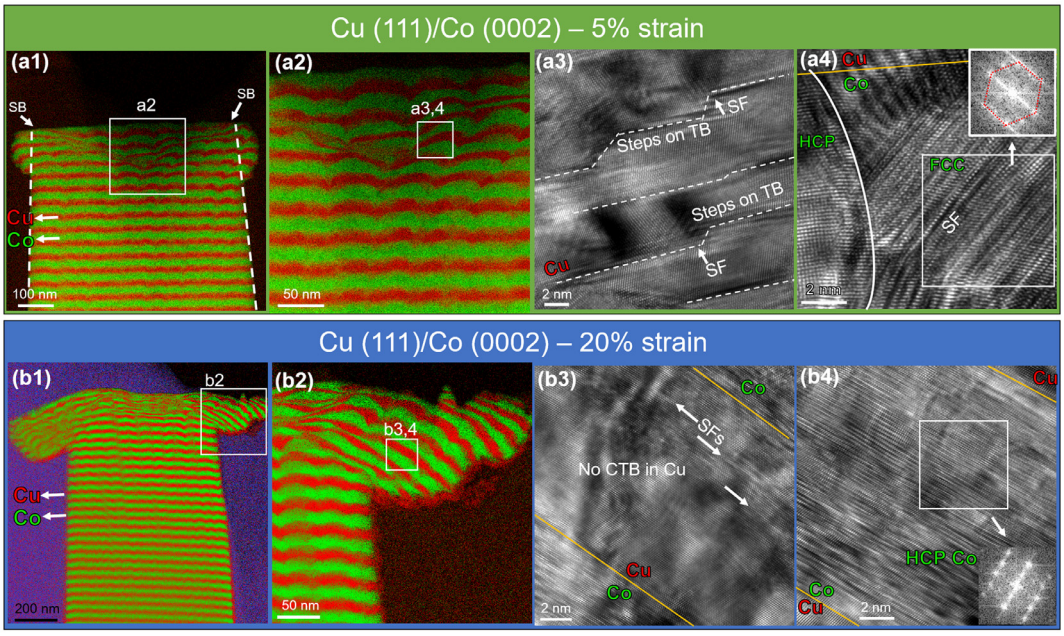

Fig. 8. XTEM micrographs and EDS maps of the Cu (111)/Co (0002) 25 nm pillar after compression. (a1-a2) EDS maps of Cu (111)/Co (0002) pillar after it is deformed to 5% true strain (100 nm compression) showing dilation of the pillar top. Shear deformation initiated from the pillar surface leads to layer rotations. (a3) Defective TBs decorated with SFs in the Cu layer. (a4) FCC Co phase with inclined SFs formed near the Cu/Co interface as confirmed by the inserted FFT. (b1-b2) EDS map of the multilayer deformed to 20% strain (400 nm compression) showing shear induced layer rotation and significant deformation (extrusion) of the pillar top. (b3, b4) HRTEM micrographs of an extruded but less deformed portion of the pillar top show prominent detwinning in the Cu layer, and high-density SFs in the HCP Co layer.

basal slip is prevented due to the small resolved shear stress (the loading direction is orthogonal to basal planes). Prismatic slip and pyramidal slip are also inhibited by the SFs on basal planes. Thus, Co layer is also strengthened by the high-density SFs. It has been frequently shown that macroscopic yielding for multilayers occurs when dislocations transmit across the layer interface [2,6,15,74-77]. In the current study, dislocation transmission across interfaces is prohibited due to slip discontinuity between HCP Co (0002) and FCC Cu (111). The collaborative defect networks inhibit the glide of dislocations in Cu and Co layer, and hinder the transmission of dislocations across layer interface, resulting in the ultra-high strength in Cu/Co nanolayers. At increasing stresses, MD simulations reveal that HCP-to-FCC phase transformation occurs in Co at the onset of yielding (Fig. 9e). The change of the nature of interface from incoherent to coherent is clearly revealed by top-down view of MD snapshots. As shown in supplementary Fig. S10, the two types of FCC (100) and (110) Cu/Co interface are dominated by FCC phase with orthogonal SFs, whereas the Cu (111)/Co (0002) interface is incoherent. During subsequent deformation, the incoherent interfaces gradually transform into FCC coherent interface decorated with inclined SFs (Fig. 10). Basically the deformation induced dislocations are able to penetrate across interface, signaled by the penetration of SFs through layer interfaces, leading to plastic yielding accompanied by a significant load-drop as shown in Fig. 9a. Subsequent deformation leads to rapid propagation of the FCC Co phase front across the HCP layer (Fig. 9f). The softening of Cu/Co system leads to significant co-deformation of Cu and Co (See supplementary video 8 for more detail). The entire process - detwinning, phase transformation and propagation of phase fronts - was also examined via dislocation analysis. Dislocation arrays are observed at the FCC Co/HCP Co phase boundaries and move with the phase boundaries during phase transformation (supplementary Fig. S11 and video 9). Thus, the MD simulation results are in excellent agreement with our post compression TEM analysis, that is the defect networks (CTB in Cu, SF in Co and FCC/HCP interface) block partial migration and prohibit slip band propagation, consequently strengthen and toughen the Cu (111)/Co (0002) multilayers.

To confirm that phase transformation indeed occurs in Cu/Co with larger individual layer thickness, we performed another set of MD simulations of Cu/Co multilayers with the same microstructure design, but with increasing individual layer thickness, 10 nm. As shown in supplementary Fig. S12, the deformation induced phase transformation is very similar to the simulated Cu/Co 5 nm multilayer.

4.3. Unique morphology and significant deformability of Cu (111)/Co (0002) pillars

Micropillar compression technique provides opportunities to discover the plastic deformation mechanisms of nanolayers, which may be difficult to decipher with nanoindentation technique alone [2]. In contrast to the slip band formation in the FCC Cu/Co multilayer systems, no slip bands were observed in the Cu (111)/Co (0002) pillars, and significant plastic deformation mainly accumulates near the top, forming a cap, while leaving the rest of the pillar largely intact.

Numerous aspects should be considered to understand such a unique morphological evolution. First, like any micropillar compression test, tapering cannot be completely eliminated, which leads to higher local stress at the top, although the tapering angle in the current study is already very small. In general, after yielding, as the top portion of the pillar gets larger, stress gradient becomes smaller and deformation starts to propagate downwards forming a barreling or reverse conical shape [35,74,78,79]. Furthermore, all three Cu/Co systems have similar degree of tapering, and thus the small tapering alone has little impact on the significant deformation of the pillar top. Second, as shown in supplementary Fig. S4 and Video 3, the significant plastic deformation in Cu (111)/Co (0002) pillars originates from dramatic strain softening of the pillar top. Strain softening of multilayers under pillar compression has been reported before [3,16,24,28,37], and is mostly

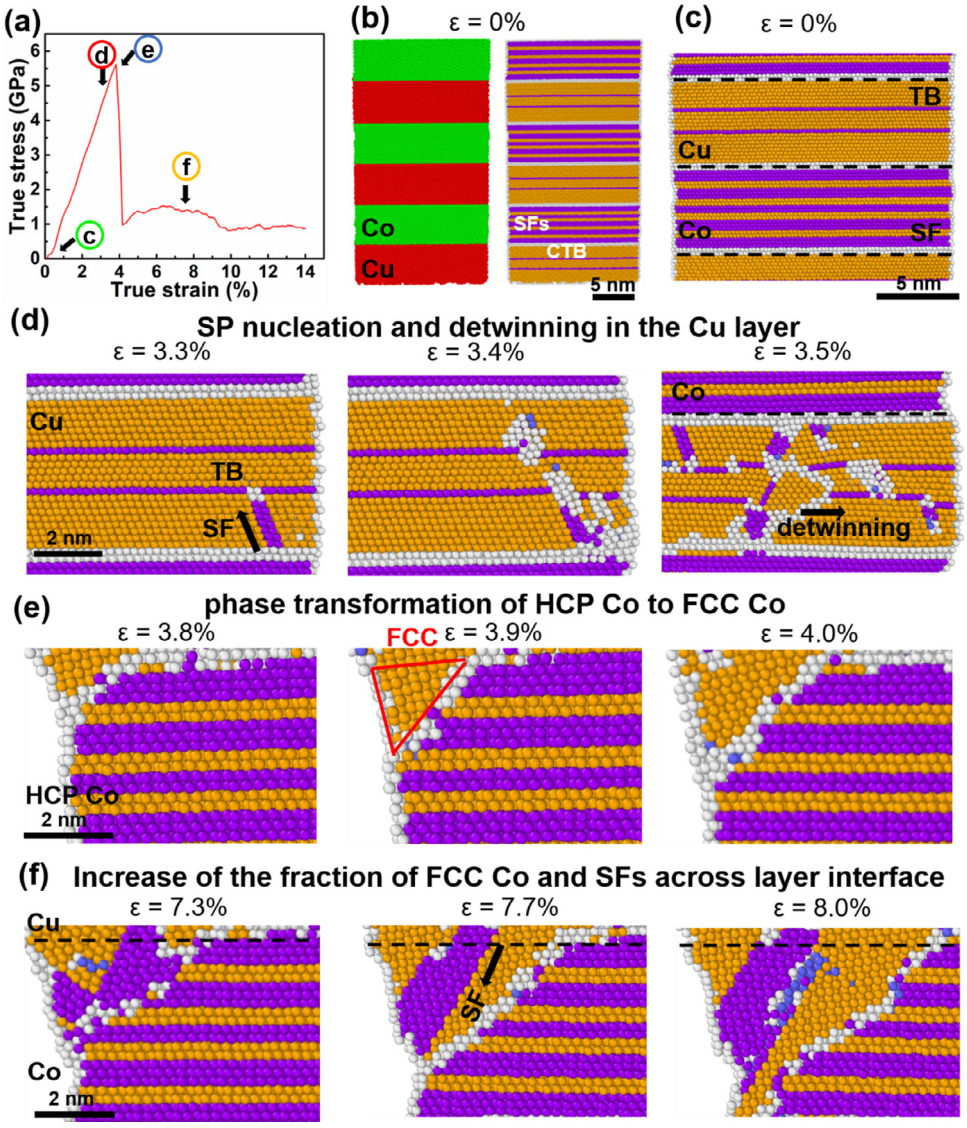

Fig. 9. MD simulation results for the compression of FCC Cu (111)/ HCP Co (0002) 5 nm nanopillars. (a) The true stress-strain curve shows the yield stress of pillars is ~ 5.5 GPa. (b) Left panel shows Cu in red and Co in green. Right panel shows atoms in FCC (orange) and HCP (purple) structure by using the common neighbor color coding. (c) Cross-section view of the model system shows the pre-existing SFs in HCP Co and TBs in FCC Cu, which are parallel to the Cu/Co interface, similar to experimental observations. (d) The nucleation of Shockley partial against TBs in Cu at 3.3% true strain. Detwinning occurred in Cu layer at 3.5% strain before yielding due to glide of Shockley partials along CTBs. (e) Phase transformation from HCP to FCC Co takes place from the pillar surface at 3.8% strain, which is at the yield point. (f) Fraction of FCC Co increases rapidly during deformation and SFs penetrate through the FCC Cu/FCC Co interface. (See supplementary video 8 for details). (For interpretation of the references to color in this figure, the reader is referred to the web version of this article.)

attributed to the effect of geometry. Non-uniaxial stress state at the corner of the pillar leads to unbalanced shear stress on different {111} planes as shown in Fig. 8a1, and subsequent layer rotation [37]. However, the geometric strain softening effect reported previously is insufficient to explain the significant plastic deformation of the pillar, and the formation of a cap layer. Significant co-deformation of Cu/Co often exceeds 90% in the top portion of deformed Cu/Co pillars, indicating the existence of superplasticity.

Third, the strain softening and significant plasticity of the cap layer arise from dominant partial dislocation activities, manifested by detwinning and phase transformation. The activation of Shockley partials leads to detwinning and softening of the Cu layer. The softening of the Cu layer also leads to the interaction of partials with incoherent layer interface and results in phase transformation in the HCP Co layer. The HCP-to-FCC phase transformation of Co leads to transparent Cu/Co layer interface and significant softening. The glide of partials on inclined {111} slip systems enables rapid propagation of FCC Co in the multilayers. Strain softening is critical to accommodate significant plasticity in the deformed pillar cap. When layer rotation occurs in the top of the pillar, the Schmid factor of the inclined slip systems would increase, thus promoting the glide of partial dislocations within the layers. In the lower portion of the pillar, there is insignificant layer rotation, and thus partials cannot be activated and the pillar retains its high resistance to plastic deformation. This unique strain softening mechanism is quite important here to enhance plasticity of the multilayers. Instead of forming shear bands or cracks like most high strength multilayer systems (supplementary Fig. S9), the softened layer would sustain a majority of plastic deformation and protect the bottom part from yielding. It is worth mentioning that although detwinning and phase transformation lead to softening in the cap layer, ultra-high stress is needed to activate such activities, leading to the observed high yield strength of Cu (111)/Co (0002) 25nm multilayer.

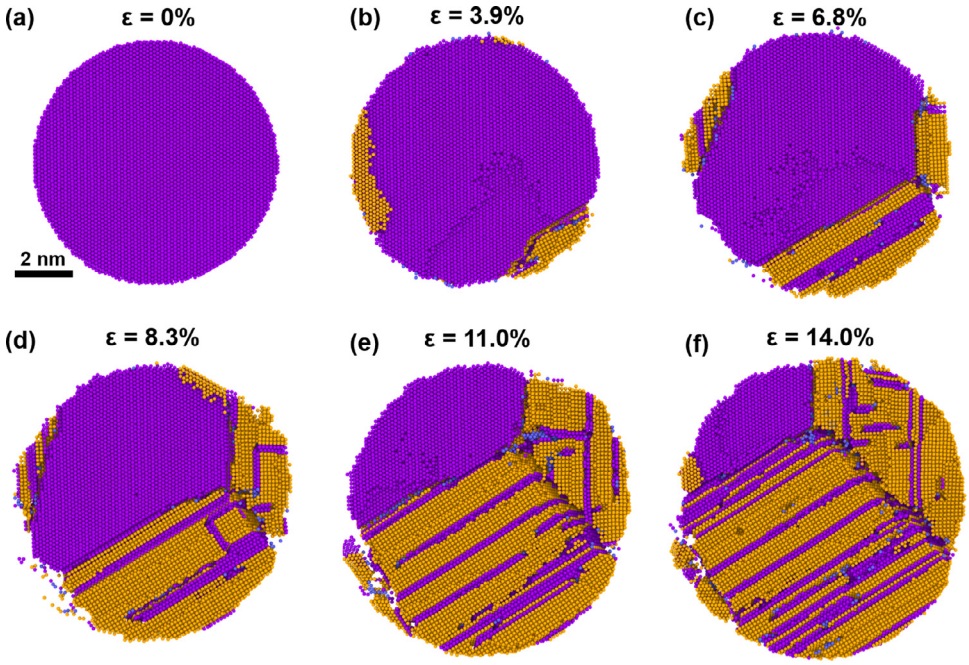

Fig. 10. Top view of the interface between Cu (111) and Co (0002) at different stress levels. Atoms are in Common Neighbor color coding, where orange is for FCC and purple is for HCP. (a) 0% strain, pure HCP phase (b) 3.9% strain, HCP Co starts to transform to FCC phase from pillar surface. (c,d) More FCC Co formed and inclined SFs are formed inside FCC phase. (e,f) More than half of HCP Co transformed to FCC Co and abundant inclined SFs formed across the interface.

Clearly more experimental and simulations work is necessary to examine the defect network enabled deformation mechanisms in future studies. The current study only unravels a corner of an exciting field, where defect network may change the deformation mechanisms and impact how we design advanced strong and deformable metallic materials. There are numerous unresolved issues, some of which are listed here. First, the influence of layer thickness on deformation mechanisms of multilayers with defect network requires further investigation. In other words, size effect on deformation mechanisms may be pivotal in conjunction with the defect networks. Second, the current MD simulations focus on a small model system limited by computational ability. Large scale MD simulations are necessary to examine the deformation mechanisms with larger layer thickness. Third, the general applicability of the defect network concept requires further validation in other systems. Defect networks that contain grain boundaries, nanovoids, phase boundaries may also operate collaboratively to enable high strength and deformability. Finally, phase transformation occurs in Co in the current study. It is unclear if phase transformation is necessary to enable high strength and plasticity in other systems with defect networks.

5. Conclusions

We report on drastically different mechanical strength and deformability of Cu/Co multilayers with identical individual layer thickness, but having three types of crystallographic orientations and layer interfaces. *In situ* micropillar compression studies show that the coherent FCC (100) and (110) Cu/Co multilayers have similar low yield strength of ~ 600 MPa and form prominent slip bands during deformation. In contrast, the incoherent Cu (111)/Co (0002) 25 nm multilayer delivers unmatched yield strength, ~ 2.4 GPa, and high flow stress, exceeding 3 GPa. The system also exhibits local superplastic deformation as evidenced by the formation of a cap layer. MD simulations reveal that the transparent FCC (100) and (110) Cu/Co interfaces are weak barriers to the transmission of dislocations or the formation of slip bands. But the superior strength in FCC/HCP Cu/Co multilayers arises from a defect network consisting of TBs, SFs and parallel incoherent layer interfaces. The plastic yielding of the FCC/HCP multilayer is due to the HCP-to-FCC phase transformations in Co. The concept of defect network described in this paper may open new avenue for the design of high-strength, deformable metallic materials.

Declaration of Competing Interest

The authors declare that they have no known competing financial interests or personal relationships that could have appeared to influence the work reported in this paper.

Acknowledgments

RS and XZ acknowledge the financial support by NSF-DMR 1642759. DN and YK acknowledge the financial support by NSF-DMR 1508484. Pillar compression and TEM analysis by SX and QL are supported by DOE-OBES under grant No. DE-SC0016337. H. Wang acknowledges the support from the U.S. Office of Naval Research (N00014-17–1–2087). Access to the Life Sciences Microscopy Center and Materials Science Microscopy Center at Purdue University are also acknowledged. The support from the Core facility for Advanced Computing and Data Science at the University of Houston is also acknowledged. We also acknowledge access to facilities at DOE Center for Integrated Nanotechnologies.

Data availability statement

The data that support the findings of this study are available from the corresponding author upon reasonable request.

Supplementary material

Supplementary material associated with this article can be found, in the online version, at doi:10.1016/j.actamat.2019.11.049.

References

[1] J. Li, Y. Chen, S. Xue, H. Wang, X. Zhang, Comparison of size dependent strengthening mechanisms in Ag/Fe and Ag/Ni multilayers, Acta Mater 114 (2016) 154–163.
[2] Y. Liu, Y. Chen, K. Yu, H. Wang, J. Chen, X. Zhang, Stacking fault and partial dislocation dominated strengthening mechanisms in highly textured Cu/Co multilayers, Int. J. Plast. 49 (2013) 152–163.
[3] I. Knorr, N.M. Cordero, E.T. Lilleodden, C.A. Volkert, Mechanical behavior of nanoscale Cu/pdsi multilayers, Acta Mater 61 (13) (2013) 4984–4995.
[4] D. Bufford, Z. Bi, Q.X. Jia, H. Wang, X. Zhang, Nanotwins and stacking faults in high-strength epitaxial ag/al multilayer films, Appl. Phys. Lett. 101 (22) (2012).
[5] J. Wang, A. Misra, An overview of interface-dominated deformation mechanisms in metallic multilayers, Curr. Opin. Solid State Mater. Sci. 15 (1) (2011) 20–28.
[6] J.Y. Zhang, X. Zhang, R.H. Wang, S.Y. Lei, P. Zhang, J.J. Niu, G. Liu, G.J. Zhang, J. Sun, Length-scale-dependent deformation and fracture behavior of cu/x (X=Nb, zr) multilayers: the constraining effects of the ductile phase on the brittle phase, Acta Mater 59 (19) (2011) 7368–7379.
[7] X.W. Zhou, R.A. Johnson, H.N.G. Wadley, Misfit-energy-increasing dislocations in vapor-deposited cofe/nife multilayers, Phys. Rev. B 69 (14) (2004) 144113.
[8] J. Wang, R.G. Hoagland, J.P. Hirth, A. Misra, Atomistic simulations of the shear strength and sliding mechanisms of copper-niobium interfaces, Acta Mater 56 (13) (2008) 3109–3119.
[9] N.A. Mara, D. Bhattacharyya, P. Dickerson, R.G. Hoagland, A. Misra, Deformability of ultrahigh strength 5nm cu/nb nanolayered composites, Appl. Phys. Lett. 92 (23) (2008).
[10] A. Misra, X. Zhang, D. Hammon, R.G. Hoagland, Work hardening in rolled nanolayered metallic composites, Acta Mater 53 (1) (2005) 221–226.
[11] A. Misra, M. Verdier, Y. Lu, H. Kung, T. Mitchell, M. Nastasi, J. Embury, Structure and mechanical properties of cu-x (X= Nb, Cr, Ni) nanolayered composites, Scr Mater 39 (4) (1998) 555–560.
[12] Y. Liu, D. Bufford, H. Wang, C. Sun, X. Zhang, Mechanical properties of highly textured Cu/Ni multilayers, Acta Mater (2011).
[13] J. McKeown, A. Misra, H. Kung, R.G. Hoagland, M. Nastasi, Microstructures and strength of nanoscale cu–ag multilayers, Scr. Mater 46 (8) (2002) 593–598.
[14] Y. Chen, Y. Liu, C. Sun, K.Y. Yu, M. Song, H. Wang, X. Zhang, Microstructure and strengthening mechanisms in Cu/Fe multilayers, Acta Mater 60 (18) (2012) 6312–6321.
[15] X. Zhang, A. Misra, H. Wang, T. Shen, M. Nastasi, T. Mitchell, J. Hirth, R. Hoagland, J. Embury, Enhanced hardening in cu/330 stainless steel multilayers by nanoscale twinning, Acta Mater 52 (4) (2004) 995–1002.
[16] P. Dayal, M.Z. Quadir, C. Kong, N. Savvides, M. Hoffman, Transition from dislocation controlled plasticity to grain boundary mediated shear in nanolayered aluminum/palladium thin films, Thin. Solid Films 519 (10) (2011) 3213–3220.
[17] W. Guo, E. Jägle, J. Yao, V. Maier, S. Korte-Kerzel, J.M. Schneider, D. Raabe, Intrinsic and extrinsic size effects in the deformation of amorphous cuzr/nanocrystalline cu nanolaminates, Acta Mater 80 (Supplement C) (2014) 94–106.
[18] J.Y. Zhang, J. Li, X.Q. Liang, G. Liu, J. Sun, Achieving optimum mechanical performance in metallic nanolayered cu/x (X = Zr, Cr) micropillars, Sci. Rep. 4 (2014) 4205.
[19] E. Fu, N. Li, A. Misra, R. Hoagland, H. Wang, X. Zhang, Mechanical properties of sputtered cu/v and al/nb multilayer films, Mater. Sci. Eng. A 493 (1) (2008) 283–287.
[20] J.M. Wheeler, R. Raghavan, V. Chawla, J. Zechner, I. Utke, J. Michler, Failure mechanisms in metal–metal nanolaminates at elevated temperatures: microcompression of cu–w multilayers, Scr. Mater 98 (2015) 28–31.
[21] Y. Kim, A.S. Budiman, J.K. Baldwin, N.A. Mara, A. Misra, S.M. Han, Microcompression study of al-nb nanoscale multilayers, J. Mater Res. 27 (3) (2012) 592–598.
[22] N. Li, M. Demkowicz, N. Mara, Y. Wang, A. Misra, Hardening due to interfacial he bubbles in nanolayered composites, Mater. Res. Lett. 4 (2) (2016) 75–82.
[23] Y. Cui, B. Derby, N. Li, N.A. Mara, A. Misra, Suppression of shear banding in high-strength cu/mo nanocomposites with hierarchical bicontinuous intertwined structures, Materials Research Letters 6 (3) (2018) 184–190.
[24] Y.Y. Lu, R. Kotoka, J.P. Ligda, B.B. Cao, S.N. Yarmolenko, B.E. Schuster, Q. Wei, The microstructure and mechanical behavior of mg/ti multilayers as a function of individual layer thickness, Acta Mater 63 (2014) 216–231.
[25] B. Ham, X. Zhang, High strength mg/nb nanolayer composites, Mater. Sci. Eng. Struct. Mater. Propert. Microstruct. Process. 528 (4–5) (2011) 2028–2033.
[26] S. Pathak, N. Velisavljevic, J.K. Baldwin, M. Jain, S. Zheng, N.A. Mara, I.J. Beyerlein, Strong, ductile, and thermally stable bcc-Mg nanolaminates, Sci. Rep. 7 (1) (2017) 8264.
[27] D. Bhattacharyya, N.A. Mara, P. Dickerson, R.G. Hoagland, A. Misra, Compressive flow behavior of al-tin multilayers at nanometer scale layer thickness, Acta Mater 59 (10) (2011) 3804–3816.
[28] S.M. Han, M.A. Phillips, W.D. Nix, Study of strain softening behavior of al-al3sc multilayers using microcompression testing, Acta Mater 57 (15) (2009) 4473–4490.
[29] C.R. Mayer, L.W. Yang, S.S. Singh, J. Llorca, J.M. Molina-Aldareguia, Y.L. Shen, N. Chawla, Anisotropy, size, and aspect ratio effects on micropillar compression of alsic nanolaminate composites, Acta Mater 114 (2016) 25–32.
[30] J.Y. Zhang, G. Liu, J. Sun, Self-toughening crystalline cu/amorphous cu–zr nanolaminates: deformation-induced devitrification, Acta Mater 66 (2014) 22–31.
[31] Z. Fan, S. Xue, J. Wang, K.Y. Yu, H. Wang, X. Zhang, Unusual size dependent strengthening mechanisms of cu/amorphous CUNB multilayers, Acta Mater 120 (2016) 327–336.
[32] Z. Fan, Q. Li, J. Li, S. Xue, H. Wang, X. Zhang, Tailoring plasticity of metallic glasses via interfaces in cu/amorphous CUNB laminates, J. Mater Res. 32 (14) (2017) 2680–2689.
[33] A. Misra, J.P. Hirth, R.G. Hoagland, Length-scale-dependent deformation mechanisms in incoherent metallic multilayered composites, Acta Mater 53 (18) (2005) 4817–4824.
[34] M.D. Uchic, D.M. Dimiduk, J.N. Florando, W.D. Nix, Sample dimensions influence strength and crystal plasticity, Science 305 (5686) (2004) 986–989.
[35] J.R. Greer, W.D. Nix, Nanoscale gold pillars strengthened through dislocation starvation, Phys. Rev. B 73 (24) (2006) 245410.
[36] J. Wang, C. Yang, P.D. Hodgson, Extrinsic size effect in microcompression of polycrystalline cu/fe multilayers, Scr. Mater 69 (8) (2013) 626–629.
[37] N.A. Mara, D. Bhattacharyya, J.P. Hirth, P. Dickerson, A. Misra, Mechanism for shear banding in nanolayered composites, Appl. Phys. Lett. 97 (2) (2010).
[38] M. Kuroda, Higher-order gradient effects in micropillar compression, Acta Mater 61 (7) (2013) 2283–2297.
[39] I.-s. Choi, Y. Gan, D. Kaufmann, O. Kraft, R. Schwaiger, Measurement of young's modulus of anisotropic materials using microcompression testing, J. Mater Res. 27 (21) (2012) 2752–2759.
[40] H. Zhang, B.E. Schuster, Q. Wei, K.T. Ramesh, The design of accurate micro–compression experiments, Scr. Mater 54 (2) (2006) 181–186.
[41] S. Plimpton, Fast parallel algorithms for short-range molecular dynamics, J. Comput. Phys. 117 (1) (1995) 1–19.
[42] G.P. Pun, Y. Mishin, Embedded-atom potential for hcp and FCC cobalt, Phys. Rev. B 86 (13) (2012) 134116.
[43] A. Stukowski, Visualization and analysis of atomistic simulation data with OVITO–the open visualization tool, Model. Simul. Mater. Sci. Eng. 18 (1) (2010) 015012.
[44] O. Anderoglu, A. Misra, H. Wang, F. Ronning, M.F. Hundley, X. Zhang, Epitaxial nanotwinned cu films with high strength and high conductivity, Appl. Phys. Lett. 93 (8) (2008).
[45] R. Su, D. Neffati, J. Cho, Q. Li, J. Ding, H. Wang, Y. Kulkarni, X. Zhang, Phase transformation induced plasticity in high-strength hexagonal close packed co with stacking faults, Scr. Mater 173 (2019) 32–36.
[46] J.S. Carpenter, A. Misra, M.D. Uchic, P.M. Anderson, Strain rate sensitivity and activation volume of cu/ni metallic multilayer thin films measured via micropillar compression, Appl. Phys. Lett. 101 (5) (2012) 051901.
[47] R.L. Schoeppner, J.M. Wheeler, J. Zechner, J. Michler, H.M. Zbib, D.F. Bahr, Coherent interfaces increase strain-hardening behavior in tri-component nano-scale metallic multilayer thin films, Mater. Res. Lett. 3 (2) (2015) 114–119.
[48] N. Li, N.A. Mara, Y.Q. Wang, M. Nastasi, A. Misra, Compressive flow behavior of cu thin films and cu/nb multilayers containing nanometer-scale helium bubbles, Scr Mater 64 (10) (2011) 974–977.
[49] A. Misra, M. Verdier, H. Kung, J.D. Embury, J.P. Hirth, Deformation mechanism maps for polycrystalline metallic multiplayers, Scr. Mater 41 (9) (1999) 973–979.
[50] S.I. Rao, P.M. Hazzledine, Atomistic simulations of dislocation–interface interactions in the cu-ni multilayer system, Philos. Mag. A 80 (9) (2000) 2011–2040.
[51] L. Lu, Y.F. Shen, X.H. Chen, L.H. Qian, K. Lu, Ultrahigh strength and high electrical conductivity in copper, Science 304 (5669) (2004) 422–426.
[52] X. Zhang, H. Wang, X.H. Chen, L. Lu, K. Lu, R.G. Hoagland, A. Misra, High-strength sputter-deposited cu foils with preferred orientation of nanoscale growth twins, Appl. Phys. Lett. 88 (17) (2006).
[53] Z.H. Jin, P. Gumbsch, K. Albe, E. Ma, K. Lu, H. Gleiter, H. Hahn, Interactions between non-screw lattice dislocations and coherent twin boundaries in face–centered cubic metals, Acta Mater 56 (5) (2008) 1126–1135.
[54] Z.W. Shan, L. Lu, A.M. Minor, E.A. Stach, S.X. Mao, The effect of twin plane spacing on the deformation of copper containing a high density of growth twins, Jom 60 (9) (2008) 71–74.
[55] L. Lu, X. Chen, X. Huang, K. Lu, Revealing the maximum strength in nanotwinned copper, Science 323 (5914) (2009) 607–610.
[56] Y. Kulkarni, R.J. Asaro, Are some nanotwinned fcc metals optimal for strength, ductility and grain stability? Acta Mater 57 (16) (2009) 4835–4844.
[57] Z.H. Jin, P. Gumbsch, E. Ma, K. Albe, K. Lu, H. Hahn, H. Gleiter, The interaction mechanism of screw dislocations with coherent twin boundaries in different face-centred cubic metals, Scr. Mater 54 (6) (2006) 1163–1168.
[58] Z.X. Wu, Y.W. Zhang, D.J. Srolovitz, Dislocation–twin interaction mechanisms for ultrahigh strength and ductility in nanotwinned metals, Acta Mater 57 (15) (2009) 4508–4518.
[59] N. Lu, K. Du, L. Lu, H.Q. Ye, Transition of dislocation nucleation induced by local stress concentration in nanotwinned copper, Nat. Commun. 6 (2015).
[60] Z. You, X. Li, L. Gui, Q. Lu, T. Zhu, H. Gao, L. Lu, Plastic anisotropy and associated deformation mechanisms in nanotwinned metals, Acta Mater 61 (1) (2013) 217–227.
[61] X.Z. Liao, Y.H. Zhao, S.G. Srinivasan, Y.T. Zhu, R.Z. Valiev, D.V. Gunderov, Deformation twinning in nanocrystalline copper at room temperature and low strain rate, Appl Phys. Lett. 84 (4) (2004) 592–594.
[62] X.H. Chen, L. Lu, Work hardening of ultrafine-grained copper with nanoscale twins, Scr. Mater 57 (2) (2007) 133–136.
[63] A.J. Cao, Y.G. Wei, Molecular dynamics simulation of plastic deformation of nanotwinned copper, J. Appl. Phys. 102 (8) (2007).
[64] A.A. Karimpoor, U. Erb, K.T. Aust, G. Palumbo, High strength nanocrystalline cobalt with high tensile ductility, Scr Mater 49 (7) (2003) 651–656.

[65] K.G. Davis, E. Teghtsoonian, Deformation twins in cobalt, Acta Metall. 10 (12) (1962) 1189–1191.
[66] W.W. Jian, G.M. Cheng, W.Z. Xu, H. Yuan, M.H. Tsai, Q.D. Wang, C.C. Koch, Y.T. Zhu, S.N. Mathaudhu, Ultrastrong mg alloy via nano-spaced stacking faults, Materials Res. Lett. 1 (2) (2013) 61–66.
[67] C. Fan, Q. Li, J. Ding, Y. Liang, Z. Shang, J. Li, R. Su, J. Cho, D. Chen, Y. Wang, J. Wang, H. Wang, X. Zhang, Helium irradiation induced ultra-high strength nanotwinned cu with nanovoids, Acta Mater 177 (2019) 107–120.
[68] N. Li, J. Wang, A. Misra, X. Zhang, J.Y. Huang, J.P. Hirth, Twinning dislocation multiplication at a coherent twin boundary, Acta Mater 59 (15) (2011) 5989–5996.
[69] J. Wang, N. Li, O. Anderoglu, X. Zhang, A. Misra, J.Y. Huang, J.P. Hirth, Detwinning mechanisms for growth twins in face-centered cubic metals, Acta Mater 58 (6) (2010) 2262–2270.
[70] J.Y. Huang, Y.K. Wu, H.Q. Ye, Phase transformation of cobalt induced by ball milling, Appl. Phys. Lett. 66 (3) (1995) 308–310.
[71] F. Delogu, Kinetics of allotropic phase transformation in cobalt powders undergoing mechanical processing, Scr. Mater 58 (2) (2008) 126–129.
[72] J. Sort, N.M. Mateescu, J. Nogués, S. Suriñach, M.D. Baró, Effect of the milling energy on the milling-induced hcp-fcc cobalt allotropic transformations, J. Metastable Nanocryst. Mater. 12 (2002) 126–133.
[73] Y.T. Zhu, X.L. Wu, X.Z. Liao, J. Narayan, L.J. Kecskés, S.N. Mathaudhu, Dislocation–twin interactions in nanocrystalline fcc metals, Acta Mater 59 (2) (2011) 812–821.
[74] J.Y. Zhang, S. Lei, Y. Liu, J.J. Niu, Y. Chen, G. Liu, X. Zhang, J. Sun, Length scale-dependent deformation behavior of nanolayered cu/zr micropillars, Acta Mater 60 (4) (2012) 1610–1622.
[75] Y.P. Li, X.F. Zhu, J. Tan, B. Wu, W. Wang, G.P. Zhang, Comparative investigation of strength and plastic instability in cu/au and cu/cr multilayers by indentation, J. Mater Res 24 (3) (2009) 728–735.
[76] A. Misra, J.P. Hirth, R.G. Hoagland, J.D. Embury, H. Kung, Dislocation mechanisms and symmetric slip in rolled nano-scale metallic multilayers, Acta Mater 52 (8) (2004) 2387–2394.
[77] A. Misra, J.P. Hirth, H. Kung, Single-dislocation-based strengthening mechanisms in nanoscale metallic multilayers, Philosoph. Mag. a-Phys. Cond. Matter Struct. Defects Mech. Propert. 82 (16) (2002) 2935–2951.
[78] J.Y. Zhang, G. Liu, J. Sun, Strain rate effects on the mechanical response in multi- and single-crystalline cu micropillars: grain boundary effects, Int. J. Plast. 50 (2013) 1–17.
[79] Z.-J. Wang, Q.-J. Li, Z.-W. Shan, J. Li, J. Sun, E. Ma, Sample size effects on the large strain bursts in submicron aluminum pillars, Appl. Phys. Lett. 100 (7) (2012) 071906.